Tobias Rudolph, Sarah Crotty, Ulrich S. Schubert and Felix H. Schacher*

Star-shaped poly(2-ethyl-2-oxazoline) featuring a porphyrin core: synthesis and metal complexation

Abstract: We demonstrate the synthesis of star-shaped poly(2-ethyl-2-oxazoline) featuring a porphyrin core starting from alkyne-functionalized porphyrin ($[TPP\text{-}TB]_4$) and azide-functionalized poly(2-ethyl-2-oxazoline) ($PEtOx\text{-}N_3$) via copper-catalyzed azide-alkyne cycloaddition (CuAAC). The porphyrin core was further utilized for the complexation of either copper or iron within the central cavity. The obtained materials were investigated using a combination of nuclear magnetic resonance spectroscopy, fourier transform infrared spectroscopy, ultraviolet-visible spectroscopy, size-exclusion chromatography, and matrix assisted laser desorption/ionization time-of-flight mass spectrometry. In the case of copper, the inclusion of the metal ion was achieved in a one-pot reaction during the CuAAC reaction for attaching the $PEtOx\text{-}N_3$ arms.

Keywords: metal-containing polymers; poly(2-ethyl-2-oxazoline); porphyrins; star-shaped polymers.

DOI 10.1515/epoly-2015-0041
Received February 17, 2015; accepted March 16, 2015; previously published online April 18, 2015

1 Introduction

For the synthesis of star-shaped polymers, typically two different approaches are used, either core first or arm first (1–3). In the case of core-first strategies, a core molecule or a multifunctional initiator is synthesized or modified with initiating groups applicable for controlled polymerization reactions. In the literature, different examples of atom transfer radical polymerization (4, 5), reversible addition fragmentation chain transfer (6), anionic ring-opening polymerization (7, 8), or cationic ring-opening polymerization (CROP) (9, 10) are reported. One clear disadvantage of the core-first approach is that complete initiation is often difficult to verify and lower arm numbers are found when compared to initiation sites. This can be avoided in the arm-first approach, as each building block can be separately characterized and the degree of functionalization can be quantitatively determined for each step. In that respect, efficient macromolecular conjugation reactions have been extensively investigated for an efficient linkage between two complementary motifs, leading to different possibilities for the synthesis of new materials (11–16). Among these possibilities, one versatile platform are copper-catalyzed azide-alkyne cycloaddition (CuAAC) reactions, which have already been used for the formation of networks (17, 18), block copolymers (19–21), or other polymer architectures (13, 22, 23).

Porphyrins show potential for use in applications such as photosensitizers (24) and catalysts (25), and, owing to an inherent high affinity for metal complexation within the porphyrin cavity, the resulting materials have attractive optical properties that render them suitable precursors for hybrid materials (6, 26–32). Moreover, polymers based on porphyrins have been studied with regard to hierarchical self-assembly processes (6, 33, 34) and to their use in selective ion complexation (4).

We were interested in the combination of functionalized porphyrins and CuAAC of suitably modified polymeric building blocks for the synthesis of symmetrical, star-shaped, porphyrin-centered polymers. For this purpose, 5,10,15,20-tetrakis(4-hydroxyphenyl)-21H,23H-porphyrin ($[TPP\text{-}OH]_4$) was equipped with alkyne functionalities, and azide-functionalized poly(2-ethyl-2-oxazoline) ($PEtOx\text{-}N_3$) was covalently attached via subsequent CuAAC chemistry. We present a detailed study of the obtained materials through a combination of nuclear magnetic resonance spectroscopy (NMR), Fourier transform infrared spectroscopy (FTIR), size exclusion chromatography (SEC), ultraviolet-visible spectroscopy (UV-Vis) and matrix assisted laser desorption/ionization time-of-flight mass spectrometry (MALDI-ToF MS). Regarding the introduction of metal ions into the porphyrin cavity, this could be achieved in a

***Corresponding author: Felix H. Schacher,** Institute of Organic Chemistry and Macromolecular Chemistry (IOMC), Friedrich Schiller University Jena, Humboldtstr. 10, 07743 Jena, Germany; and Jena Center for Soft Matter (JCSM), Friedrich Schiller University Jena, Philosophenweg 7, 07743 Jena, Germany,
e-mail: felix.schacher@uni-jena.de
Tobias Rudolph, Sarah Crotty and Ulrich S. Schubert: Institute of Organic Chemistry and Macromolecular Chemistry (IOMC), Friedrich Schiller University Jena, Humboldtstr. 10, 07743 Jena, Germany; and Jena Center for Soft Matter (JCSM), Friedrich Schiller University Jena, Philosophenweg 7, 07743 Jena, Germany

one-pot synthesis for copper, whereas the introduction of iron (III) was realized in two steps.

2 Results and discussion

Herein, we focus on the synthesis of star-shaped poly(2-ethyl-2-oxazoline) (PEtOx) featuring a porphyrin core and four PEtOx arms via the arm-first approach. After the synthesis of azide-functionalized PEtOx building blocks, subsequent CuAAC reactions were used for the formation of star-shaped polymers. Our motivation is that well-defined porphyrin-centered building blocks with side chains of different lengths might be used as unimolecular sensors or in self-assembly studies owing to the planar nature of the porphyrin core. In that respect, we have already shown that the self-assembly mechanism for ABA bolaamphiphiles can be controlled by adjusting the length of the solubilizing PEtOx side chain in oligophenyleneethylene-based materials (35).

Commercially available $[TPP\text{-}OH]_4$ was used as a starting material for the preparation of an alkyne-functionalized core ($[TPP\text{-}TB]_4$). By etherification of the four hydroxyl groups, alkyne-functionalized $[TPP\text{-}TB]_4$ could be synthesized, where TB refers to the alkyne moieties (Figure 1A; Scheme S1). Briefly, $[TPP\text{-}OH]_4$ was dissolved in a tetrahydrofuran/methanol mixture (THF/MeOH; 5:1; v/v) together with potassium carbonate (K_2CO_3) and propargyl bromide and stirred at 45°C overnight. After the purification, $[TPP\text{-}TB]_4$ was obtained and investigated via NMR and FTIR, confirming the formation of the desired product in an overall yield of 95% (Figures S1 and S2). Full conversion of the hydroxyl group was proven by ^1H NMR through the disappearance of the corresponding signal at ≈10 ppm, whereas the aromatic signals for the phenyl ring were shifted by 0.1 ppm to lower field (Figure S1). The pyrrole NH signal of the porphyrin appeared at -2.8 ppm, which remained constant, and new signals corresponding to the alkyne functionality appeared at 5.1 and 3.8 ppm. Through FTIR, the disappearance of a broad peak for the hydroxyl group in the range above ≈3000 cm^{-1} and the appearance of a new signal corresponding to alkyne C-H (at 3290 cm^{-1}) and at 1025 cm^{-1} for a C-O stretching vibration could be observed (Figure S2). The characterization via NMR and FTIR confirmed the successful synthesis of $[TPP\text{-}TB]_4$. The solution properties of the pristine $[TPP\text{-}OH]_4$ and $[TPP\text{-}TB]_4$ were investigated via UV-Vis in THF. As can be seen in Figure S3, the shape, distribution, and intensity ratio of the absorption maxima remained

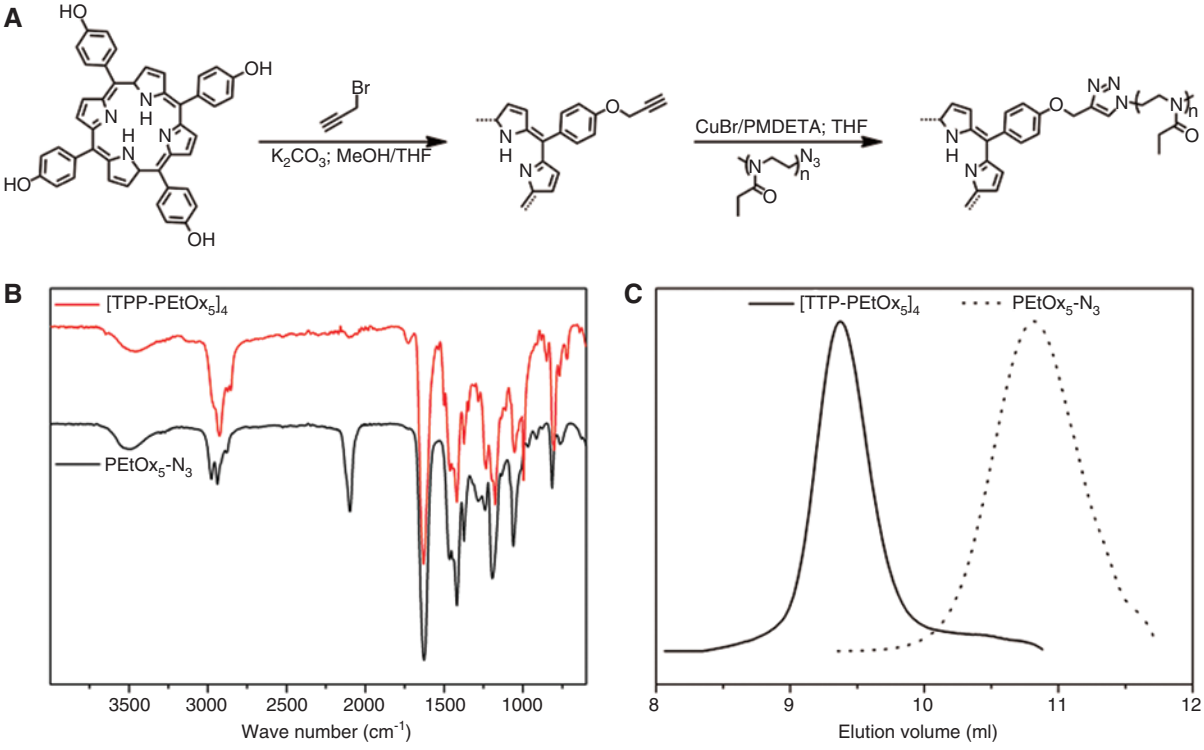

Figure 1: (A) Alkyne modification of $[TPP\text{-}OH]_4$ via etherification with propargyl bromide and subsequent CuAAC chemistry with $PEtOx_5\text{-}N_3$, forming porphyrin-centered star-shaped $[TPP\text{-}PEtOx_5]_4$; (B) comparison of FT-IR spectra for $PEtOx_5\text{-}N_3$ (black trace) and $[TPP\text{-}PEtOx_5]_4$ after purification (red trace); (C) comparison of SEC traces for $PEtOx_5\text{-}N_3$ (dotted line) and $[TPP\text{-}PEtOx_5]_4$ after precipitation (straight line).

constant before and after the modification, showing an intensive Soret band at 421 nm, whereas further bands were observed at 549, 554, 595, and 653 nm, respectively. This observation led us to the assumption that the optical properties were not changed during this modification step and that the integrity of the functionalized porphyrin unit was confirmed.

For the synthesis of azide-functionalized PEtOx oligomers, 2-ethyl-2-oxazoline (EtOx) was polymerized via microwave-assisted CROP initiated via methyl *p*-toluenesulfonate (MeTos) in acetonitrile (ACN). The reaction was terminated by the addition of sodium azide (NaN_3), leading to a substitution reaction introducing an azide end group (Scheme S2) (35). For the polymerization, a monomer-to-initiator ratio ([M]/[I]) of 5 at a constant monomer concentration of 4 mol l^{-1} was placed in the microwave synthesizer at 140°C. The obtained oligomer was investigated via NMR, SEC, and FTIR, to determine the degree of functionalization and molar mass (Figures S4–S6), and was found to be $PEtOx_5$-N_3 (the subscript denotes the degree of polymerization). The degree of functionalization seems to be quantitatively as no aromatic signals, corresponding to the tosyl group, were observed via ^{1}H NMR after azide modification (Figure S4).

For the synthesis of a symmetrical, star-shaped, porphyrin-centered $[TPP\text{-}PEtOx_5]_4$, CuAAC reactions were chosen as a versatile platform (Figure 1A). For this purpose, 1.5 eq. of $PEtOx_5$-N_3 in comparison to the alkyne functionalities of core ($[TPP\text{-}TB]_4$) was dissolved in THF. $PEtOx_5$-N_3 was used in a slight excess to ensure full conversion of the alkyne functionalities. The solution was purged with argon for 5 min, while copper bromide (CuBr; 1.5 eq.) and *N*,*N*′,*N*″,*N*″-pentamethyldiethylenetriamine (PMDETA; 1.5 eq.) were added under an argon stream. The solution was heated to 80°C in an oil bath for 10 min, passed over an aluminum oxide (AlOx N) column to remove the copper, and precipitated into diethyl ether. The purple precipitate was filtered and dried under vacuum, obtaining $[TPP\text{-}PEtOx_5]_4$ as a purple polymer, while any excess of $PEtOx_5$-N_3 remained in solution.

$[TPP\text{-}PEtOx_5]_4$ was investigated via SEC, FTIR, UV-Vis, NMR, and MALDI-ToF MS. Through SEC, a clear shift of the elution trace (straight line) to lower elution volume in comparison to $PEtOx_5$-N_3 (dashed line) could be observed (Figure 1C), indicating the absence of free linear polymer after purification. Through FTIR, a complete disappearance of the azide signal (≈2100 cm^{-1}) confirmed full conversion of $PEtOx_5$-N_3 (Figure 1B).

UV-Vis spectra (Figure 2B; Figure S7) of $[TPP\text{-}TB]_4$ and $[TPP\text{-}PEtOx_5]_4$ in THF showed differences in the Q-band region, whereas the Soret band remained at the same position. The individual signals at 519 and 554 nm ($[TPP\text{-}TB]_4$) collapsed into one signal at 542 nm, which has been described for the complexation of metal ions in the center of the phthalocyanine cavity (36). This led to the assumption that, during the CuAAC reaction, a copper complex with porphyrin was formed ($[Cu\text{-}TPP\text{-}PEtOx_5]_4$). NMR measurements showed no signals for the porphyrin units in the aromatic region, presumably due to the ferromagnetic character of the copper ions (Figure S8). This effect was also observed in the case of non-symmetrically substituted porphyrins and could be reduced by the addition of a ligand to minimize the magnetic exchange interactions between Cu-Cu ions (29). In our case, both UV-Vis and NMR indicated the incorporation of Cu ions into the cavity of the porphyrin core for $[TPP\text{-}PEtOx_5]_4$. The formation of this Cu complex also occurred under different reaction conditions for the CuAAC step (80°C for 5–10 min, room temperature for <12 h).

For the synthesis of a metal-free $[TPP\text{-}PEtOx_5]_4$, $[Cu\text{-}TPP\text{-}PEtOx_5]_4$ was dissolved in neat sulfuric acid and stirred for 12 h at room temperature (28). Acid-catalyzed hydrolysis of PEtOx (37–39) under these conditions was not observed in NMR spectra. Afterwards, no significant change in the elution behavior was observed in SEC (Figure 2C; Table 1). Nevertheless, comparable UV-Vis spectra as for earlier described $[TPP\text{-}TB]_4$ were observed, hinting towards the successful removal of copper from the porphyrin cavity and the formation of $[TPP\text{-}PEtOx_5]_4$. More precisely, both the ratio and the position of the signals, in particular in the case of the bands at 519 and 554 nm, coincided with the measurements for $[TPP\text{-}TB]_4$ (Figure 2D; see Figure S10).

The incorporation of different metal ions into porphyrin cavities has been described in the literature (30, 40). Because of the similarity of porphyrin and hemoglobin as iron-centered porphyrin-based complexes, we were interested in whether iron(III) ions could be selectively introduced, leading to $[Fe\text{-}TPP\text{-}PEtOx_5]_4$. Direct exchange by heating $[Cu\text{-}TPP\text{-}PEtOx_5]_4$ in the presence of iron (III) chloride ($FeCl_3$) at 90°C for 24 h was not successful, presumably due to the strong complexation of the copper ion. Using $[TPP\text{-}PEtOx_5]_4$ for the inclusion of iron into the cavity was not successful either, as the remaining acid might lead to the direct removal of the iron again. Therefore, the inclusion of iron into $[TPP\text{-}PEtOx_5]_4$ was achieved by the synthesis of an iron-containing core ($[Fe\text{-}TPP\text{-}TB]_4$), which was prepared by direct addition of iron(III) chloride to $[TPP\text{-}TB]_4$. After 24 h at 80°C, $[Fe\text{-}TPP\text{-}TB]_4$ was obtained after purification in a yield of 54% (Figures S12 and S13). Because of the ferromagnetic character of iron(III), characterization via NMR was not possible and FTIR was

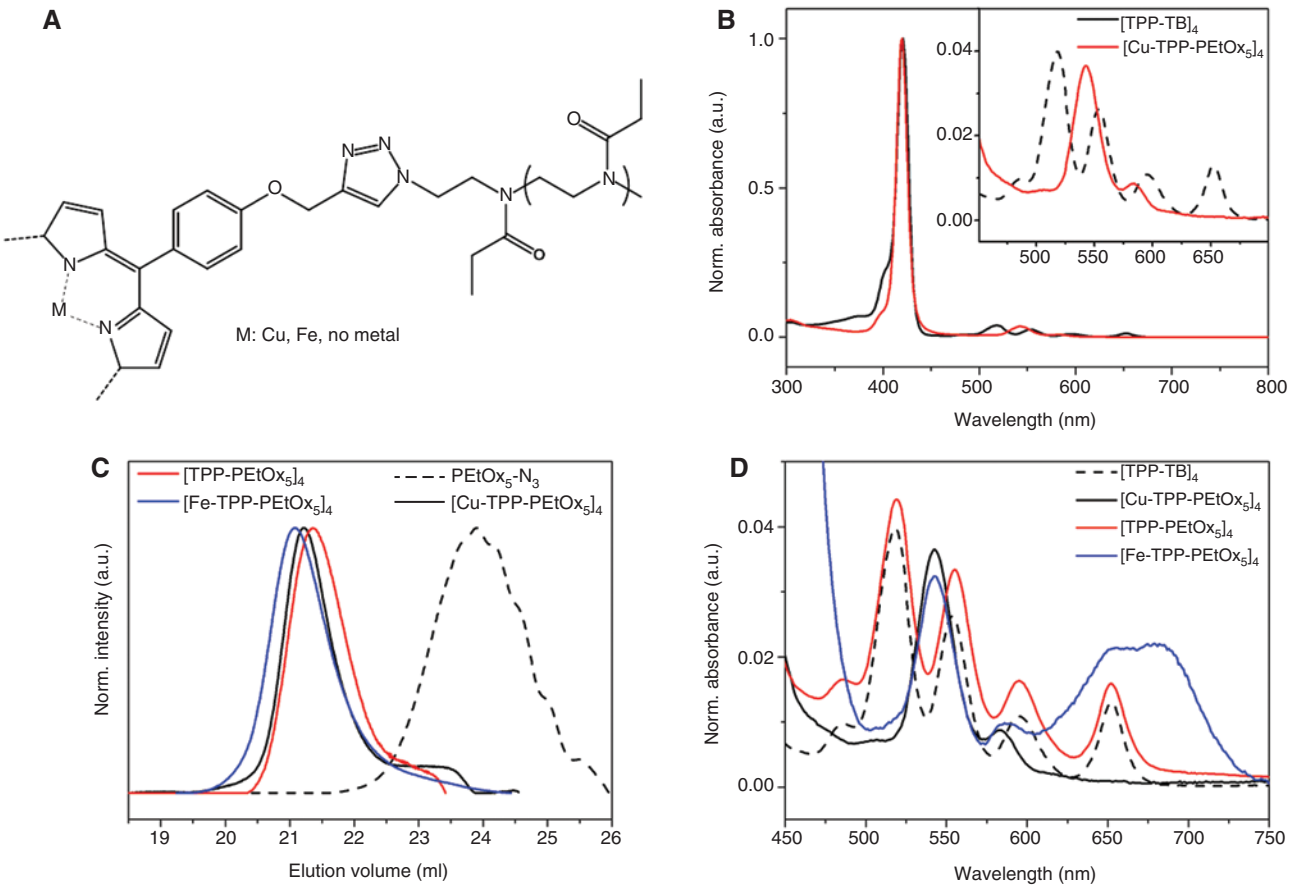

Figure 2: (A) Structure of $[Me\text{-}TPP\text{-}PEtOx_5]_4$; (B) comparison of UV-Vis spectra for $[TPP\text{-}TB]_4$ (black dashed line) and $[Cu\text{-}TPP\text{-}PEtOx_5]_4$; (C) comparison of SEC traces for $PEtOx_5\text{-}N_3$ (dashed line), $[Cu\text{-}TPP\text{-}PEtOx_5]_4$ (black line), $[Fe\text{-}TPP\text{-}PEtOx_5]_4$ (blue line), and $[TPP\text{-}PEtOx_5]_4$ (red line); (D) comparison of UV-Vis spectra for $[TPP\text{-}TB]_4$ (black dashed line), $[Cu\text{-}TPP\text{-}PEtOx_5]_4$ (straight black line), $[TPP\text{-}PEtOx_5]_4$ (red line), and $[Fe\text{-}TPP\text{-}PEtOx_5]_4$ (blue line).

applied instead. Compared to the FTIR of $[TPP\text{-}TB]_4$, that of $[Fe\text{-}TPP\text{-}TB]_4$ showed differences in the region associated with pyrrole moieties in the range of 1300 to 900 cm^{-1}, in particular at 995 cm^{-1} (Figure S12). Subsequently, $[Fe\text{-}TPP\text{-}TB]_4$ was used for CuAAC reactions with $PEtOx_5\text{-}N_3$ as described earlier. After precipitation, $[Fe\text{-}TPP\text{-}PEtOx_5]_4$ was characterized via SEC and FTIR, which showed an elution behavior comparable to those of $[Cu\text{-}TPP\text{-}PEtOx_5]_4$ and $[TPP\text{-}PEtOx_5]_4$ (Figure 2C; Table 1; Figure S16). Upon direct comparison of the FTIR spectra for $[Fe\text{-}TPP\text{-}PEtOx_5]_4$, $[Cu\text{-}TPP\text{-}PEtOx_5]_4$, and $[TPP\text{-}PEtOx_5]_4$, a signal, which can be attributed to pyrrole-metal complexes, being formed could be found at 995 cm^{-1}, whereas this individual signal disappeared in the case of $[TPP\text{-}PEtOx_5]_5$ (Figure S17).

Furthermore, the UV-Vis spectrum for $[Fe\text{-}TPP\text{-}PEtOx_5]_4$ in comparison to that for $[Cu\text{-}TPP\text{-}PEtOx_5]_4$ also showed a combined band at 542 nm, indicating metal complexation, and a new broad signal from 600 to 750 nm (Figure S14). The second broad signal was also indicated by the brownish color of the obtained material. As $[Fe\text{-}TPP\text{-}PEtOx_5]_4$ shows certain similarity to hemoglobin, selective complexation of oxygen by $[Fe\text{-}TPP\text{-}PEtOx_5]_4$ when stored under air can be assumed. This was already observed in SEC for $[Fe\text{-}TPP\text{-}PEtOx_5]_4$ after several days, where an additional distribution at higher molar masses could be found, which might indicate the presence of partially bridged or

Table 1: Selected characterization data of linear and star-shaped porphyrin-centered polymers synthesized in this study.

Polymer	M_n [a] (g mol^{-1})	$Đ$ [a]	M_p [b] (g mol^{-1})
$PEtOx_5\text{-}N_3$	710	1.37	
$[TPP\text{-}PEtOx_5]_4$	4600	1.12	2965
$[Cu\text{-}TPP\text{-}PEtOx_5]_4$	4900	1.10	3004
$[Fe\text{-}TPP\text{-}PEtOx_5]_4$	5100	1.14	2996
$[Cu\text{-}TPP\text{-}PEtOx_{11}]_4$	6100[c]	1.12	4700
$[Cu\text{-}TPP\text{-}PEtOx_{15}]_4$	8800[c]	1.07	6400

[a]SEC (DMAC/LiCl) PS calibration.
[b]MALDI-ToF MS.
[c]SEC ($CHCl_3$/TEA/iPrOH) PS calibration.

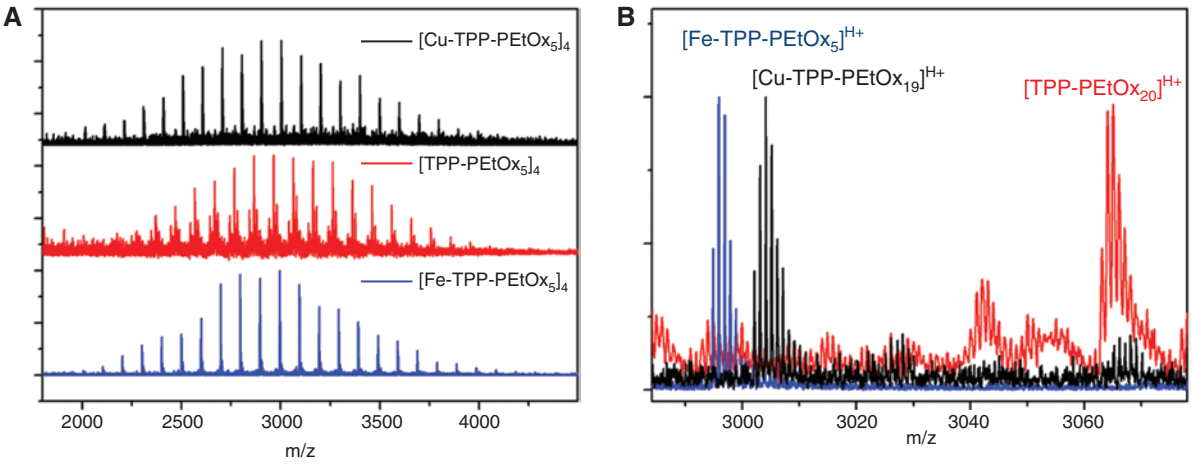

Figure 3: (A) Comparison of MALDI-ToF MS spectra for $[Cu\text{-}TPP\text{-}PEtOx_5]_4$ (black trace), $[TPP\text{-}PEtOx_5]_4$ (red trace), and $[Fe\text{-}TPP\text{-}PEtOx_5]_4$ (blue trace); (B) comparison of the major peak measured by MALDI-ToF MS spectra for $[Fe\text{-}TPP\text{-}PEtOx_{19}]$ (blue trace), $[Cu\text{-}TPP\text{-}PEtOx_{19}]$ (black trace), and $[TPP\text{-}PEtOx_{20}]$ (red curve).

oxidized $[Fe^{ox}\text{-}TPP\text{-}PEtOx_5]_4$ (Figure S18A). Oxidation or a low solubility of $[Fe\text{-}TPP\text{-}TB]_4$ might also explain the broad absorption bands in the UV-Vis spectra (Figure S13) at ≈375 and 490 nm. The solubility in the case of $[Fe\text{-}TPP\text{-}PEtOx_5]_4$ in THF increased in comparison to that of $[Fe\text{-}TPP\text{-}TB]_4$ by the attached polymer chains, and, presumably, both oxidation and aggregation decreased in THF.

We additionally subjected $[Fe\text{-}TPP\text{-}PEtOx_5]_4$, $[Cu\text{-}TPP\text{-}PEtOx_5]_4$, and $[TPP\text{-}PEtOx_5]_4$ to MALDI-ToF MS. The overall molar mass obtained for $[Fe\text{-}TPP\text{-}PEtOx_5]_4$, $[Cu\text{-}TPP\text{-}PEtOx_5]_4$, and $[TPP\text{-}PEtOx_5]_4$ could be determined at around 3000 g mol^{-1}, respectively, which is in good agreement with the desired composition (Figure 3A; Table 1). The calculated and measured isotopic patterns both showed differences corresponding to the according cavity-metal-intercalations (Figure 3B). In Figure 3B, the overlay shows a clear difference between the spectra for one peak corresponding to the same number of PEtOx arms, and the cationization agent of the individual star-macromolecules is illustrated, which shows a dependency on the specific composition. Depending on the incorporated metal for the porphyrin stars, shifts in the molar mass distributions were determined. The calculated isotopic patterns and the experimental data from MS for $[Fe\text{-}TPP\text{-}PEtOx_5]_4$, $[Cu\text{-}TPP\text{-}PEtOx_5]_4$, and $[TPP\text{-}PEtOx_5]_4$ fit, taking into account the architecture and ionization of the macromolecules (Figures S9, S11, and S15). Moreover, $[Fe^{ox}\text{-}TPP\text{-}PEtOx_5]_4$ showed at least two molar mass distributions at 3500 and 5000 g mol^{-1}, indicating bridging between two $[Fe\text{-}TPP\text{-}PEtOx_5]_4$ macromolecules.

The aforementioned outlined concept of the synthesis of star-shaped $[TPP\text{-}PEtOx_x]_4$ materials can also be applied for side chains with higher molar mass. Exemplarily, this has been shown using $PEtOx_{11}\text{-}N_3$ and $PEtOx_{15}\text{-}N_3$ as azide-functionalized building blocks. Comparable one-pot CuAAC reactions led to the formation of $[Cu\text{-}TPP\text{-}PEtOx_x]_4$ star-shaped polymers (Figure S19; Table 1).

3 Conclusion

Well-defined star-shaped polymers featuring a porphyrin core and PEtOx side chains of different lengths can be readily synthesized using CuAAC chemistry starting from alkyne-functionalized porphyrin and azide-functionalized poly(2-ethyl-2-oxazoline) ($PEtOx\text{-}N_3$). Mass spectrometry was used to investigate material characteristics as well as the intercalation of copper or iron into the porphyrin cavity of $[TPP\text{-}PEtOx_5]_4$ in addition to UV-Vis and FTIR. Such well-defined hybrid building blocks with defined amounts of metal cations are promising materials for future self-assembly studies. Another interesting feature is the herein observed susceptibility of $[Fe\text{-}TPP\text{-}PEtOx_5]_4$ to oxidation in the presence of oxygen.

4 Materials and methods

4.1 Methods

4.1.1 Nuclear magnetic resonance spectroscopy

Proton nuclear magnetic resonance (^{1}H NMR) spectra were recorded in $CDCl_3$ on a Bruker AC 300-MHz spectrometer at 298 K. Chemical shifts are given in parts per million (ppm, δ scale) relative to the residual signal of the deuterated solvent.

4.1.2 Size-exclusion chromatography

Size-exclusion chromatography was performed on a Agilent (Agilent Technology, Waldbronn, Germany) system equipped with an SCL-10A system controller, an G1329A pump, an G1362A refractive index detector, and both a PSS Gram30 and a PSS Gram1000 column series, whereby *N,N*-dimethylacetamide (DMAC) with 5 mmol of LiCl was used as an eluent at 1 ml min^{-1} of flow rate and the column oven was set to 40°C. The system was calibrated using polystyrene (PS; 100–1,000,000 g mol^{-1}) standards. Furthermore, a Shimadzu (Shimadzu, Duisburg, Germany) equipped with an SCL-10A system controller, an LC-10AD pump, and an RID-10A refractive index detector using a solvent mixture containing chloroform ($CHCl_3$), triethylamine (TEA), and *iso*-propanol (*i*-PrOH) (94:4:2) at a flow rate of 1 ml min^{-1} on a PSS SDV linear M 5-µm column at 40°was used for the investigation of the polymers.

4.1.3 Fourier-transform infrared spectroscopy

Dry powders of the copolymers were directly placed on the crystal of the ATR-FTIR (Affinity-1 FTIR, Shimadzu) or ATR-FT-IR (ALPHA's Platinum ATR, Bruker) for measurements in the range of 4000 to 600 cm^{-1}.

4.1.4 Microwave-assisted polymerizations

Microwave-assisted polymerizations were carried out utilizing an Initiator Sixty single-mode microwave synthesizer (Biotage, Uppsala, Sweden) equipped with a noninvasive IR sensor (accuracy: 2%). Microwave vials (conical, 0.5–2 ml) were heated at 110°C overnight and allowed to cool to room temperature under nitrogen atmosphere. All polymerizations were carried out using temperature control.

4.1.5 Matrix-assisted laser desorption ionization time-of-flight mass spectrometer

Matrix-assisted laser desorption/ionization time-of-flight mass spectrometry was performed on an Ultraflex III TOF/TOF (Bruker Daltonics, Bremen, Germany) equipped with a Nd:YAG laser and without any matrix and using NaCl as a doping agent in reflector and linear mode. The instrument was calibrated prior to each measurement following an external PMMA standard from PSS Polymer Standards Services GmbH (Mainz, Germany).

4.1.6 UV-Vis Spectroscopy

UV-Vis absorption spectra were recorded on a Specord 250 spectrometer (Analytik Jena, Jena, Germany) in Suprasil quartz glass cuvettes (104-QS, Hellma Analytics) with a thickness of 10 mm. The temperature at the measurements was controlled by a Jumo dTRON 08.1 instrument (Analytik Jena).

4.2 Materials

5,10,15,20-Tetrakis(4-hydroxyphenyl)-21H,23H-porphine (TPP), potassium carbonate, sodium azide, iron (III) chloride, and propargyl bromide (80 wt.% in toluene) were purchased from Sigma Aldrich. Propargyl bromide was distilled from $CaCl_2$ and stored under argon. 2-Ethyl-2-oxazoline was distilled from barium oxide under vacuum and stored under argon in a glove box.

4.2.1 Synthesis of alkyne modified tetrakisphenylporphyrin (TB-TPP)

5,10,15,20-Tetrakis(4-hydroxyphenyl)-21*H*,23*H*-porphyrin (TPP, 500 mg, 0.734 mmol) was dissolved in a solvent mixture of tetrahydrofuran and methanol (15 ml THF and 3 ml MeOH) together with 1.5 g of potassium carbonate (10.85 mmol). Propargyl bromide (3 ml, 26.9 mmol) was added to the solution under vigorous stirring and stirred for 24 h at 45°C. The solvent was removed under reduced pressure, dissolved in THF (concentrated), filtered, and dried under vacuum to obtain a purple solid. Yield: 95%, 590 mg.

^{1}H NMR (300 MHz, DMSO): 8.85 (s, pyrrole protons), 8.15 (d, phenyl), 7.43 (d, phenyl), 5.10 (s, -C*H*$_2$-C-CH), 3.77 (s, -CH$_2$-C-C*H*), -2.91 (s, -N*H*-) ppm.

FT-IR: 3290 (-CH), 1025 (C-O-C) cm^{-1}.

4.2.2 Synthesis of alkyne-modified iron(III) containing tetrakisphenylporphyrin ([Fe-TPP-TB]$_4$)

TB-TPP (92 mg, 0.11 mmol) was dissolved together with iron(III) chloride ($FeCl_3$, 52 mg, 0.19 mmol) in a THF/methanol mixture (10:4, v/v) and heated in an oil bath at 90°C overnight. The reaction mixture was diluted with dichloromethane and extracted with water, and the organic phase was dried over sodium sulfate, filtered, and then dried under vacuum. The product was obtained as a brownish solid. Yield: 54%, 54 mg.

ATR-FT-IR: 3300 (-CH), 1017 (C-O-C), 995 (pyrrole-metal) cm^{-1}.

4.2.3 Synthesis of azide-functionalized $PEtOx_5$-N_3

Methyl *p*-toluenesulfonate and EtOx were dissolved in ACN at a monomer-to-initiator ratio ([M]/[I]) of 5 and at a monomer concentration of 4 mol l^{-1}. The capped vials were placed in a microwave synthesizer at 140°C. The polymerization was terminated via the addition of dried sodium azide under inert conditions. The polymers were obtained after filtering the excess sodium azide and washing with dichloromethane; the organic phase was dried under vacuum. After precipitation in cold diethyl ether, the polymer was filtered and dried under vacuum.

SEC ($CHCl_3$/*i*-PrOH/Et_3N): M_n=900 g mol^{-1}; $Đ$=1.12 (PS calibration). SEC (DMAC/LiCl): M_n=710 g mol^{-1}; $Đ$=1.37 (PS calibration).

^{1}H NMR (300 MHz, $CDCl_3$, δ): 3.6–3.2 (br, -N-CH_2-CH_2-), 2.5–2.2 (br, CO-CH_2-CH_3), 1.2–0.9 (br, CO-CH_2-CH_3) ppm.

ATR-FT-IR: 2096 (azide), 1630 (carbonyl) cm^{-1}.

4.2.4 CuAAC reaction between $[TPP\text{-}TB]_4$ and azide-modified PEtOx ($PEtOx_5$-N_3) forming $[Cu\text{-}TPP\text{-}PEtOx_5]_4$

The core ($[TPP\text{-}TB]_4$) and $PEtOx_5$-N_3 (6 eq.) were dissolved in THF. The solution was purged with argon for 5 min, while CuBr (6 eq.) and PMDETA (6 eq.) were added under argon stream. The solution was heated up to 80°C in an oil bath for 10 min, diluted with chloroform, and passed over an aluminum oxide (AlOx N) column to remove the copper. The solvent was removed under reduced pressure and precipitated in cold diethyl ether. The purple precipitate was filtered and dried under vacuum, obtaining the porphyrin-centered polymer.

SEC (DMAC/LiCl): M_n=4900 g mol^{-1}; $Đ$=1.10 (PS calibration).

^{1}H NMR (300 MHz, $CDCl_3$, δ): 8.0–7.65 (tetrazine), 5.5-5.2 (tetrazine-CH_2-CH_2-), 4.8–4.6 (tetrazine-CH_2-O-), 4.0–3.8 (tetrazine-CH_2-CH_2-), 3.8–3.1 (backbone), 2.5–2.2 (br, CO-CH_2-CH_3), 1.2–0.9 (br, CO-CH_2-CH_3) ppm.

ATR-FT-IR: 1630 (carbonyl), 995 (pyrrole-metal) cm^{-1}.

4.2.5 Synthesis of metal-free $[TPP\text{-}PEtOx_5]_4$

For the synthesis of metal-free $[TPP\text{-}PEtOx_5]_4$, $[Cu\text{-}TPP\text{-}PEtOx_5]_4$ was dissolved in concentrated sulfuric acid and stirred at room temperature for 24 h. The product was obtained after dilution with water (caution during the addition of water to sulphuric acid) and then extracted with dichloromethane and water, dried under vacuum, and precipitated in diethyl ether.

SEC (DMAC/LiCl): M_n=4600 g mol^{-1}; $Đ$=1.12 (PS calibration).

^{1}H NMR (300 MHz, $CDCl_3$, δ): 8.0–7.65 (tetrazine), 5.7-5.4 (tetrazine-CH_2-CH_2-), 4.8–4.6 (tetrazine-CH_2-O-), 4.0–3.8 (tetrazine-CH_2-CH_2-), 3.8–3.1 (backbone), 2.5–2.2 (br, CO-CH_2-CH_3), 1.2–0.9 (br, CO-CH_2-CH_3) ppm.

ATR-FT-IR: 1630 (carbonyl) cm^{-1}.

4.2.6 CuAAC reaction between $[Fe\text{-}TPP\text{-}TB]_4$ and azide-modified PEtOx ($PEtOx_5$-N_3) forming $[Fe\text{-}TPP\text{-}PEtOx_5]_4$

The core ($[Fe\text{-}TPP\text{-}TB]_4$) and $PEtOx_5$-N_3 (6 eq.) were dissolved in THF. The solution was purged with argon for 5 min, while CuBr (6 eq.) and PMDETA (6 eq.) were added under argon stream. The solution was heated up to 80°C in an oil bath for 10 min, diluted with chloroform, and passed over an aluminum oxide (AlOx N) column to remove the copper. The solvent was removed under reduced pressure and precipitated in cold diethyl ether. The brownish precipitate was filtered and dried under vacuum, obtaining the porphyrin-centered polymer.

SEC (DMAC/LiCl): M_n=5100 g mol^{-1}; $Đ$=1.14 (PS calibration).

ATR-FT-IR: 1630 (carbonyl), 995 (pyrrole-metal) cm^{-1}.

Acknowledgments: F.H.S. thanks the VCI for an independent researcher fellowship, and T.R. the Carl-Zeiss foundation for a PhD scholarship. F.H.S. and U.S.S. also acknowledge the Thuringian Ministry for Education, Science and Culture (grant nos.: B514-09051 and B715-08011, NanoConSens; B515-10065, ChaPoNano) for financial support. T.R. would like to thank Katrin Knop for scientific discussions concerning TPP, as well as Benjamin Kintzel and Martin Obst for help during laboratory courses. We thank Bruker Daltonics for their help and support.

References

1. Pitsikalis M, Pispas S, Mays J, Hadjichristidis N. Nonlinear block copolymer architectures. Adv Polym Sci. 1998;135:1–137.
2. Hadjichristidis N, Iatrou H, Pitsikalis M, Mays J. Macromolecular architectures by living and controlled/living polymerizations. Prog Polym Sci. 2006;31(12):1068–32.
3. Blencowe A, Tan JF, Goh TK, Qiao GG. Core cross-linked star polymers via controlled radical polymerisation. Polymer 2009;50(1):5–32.

4. High LRH, Holder SJ, Penfold HV. Synthesis of star polymers of styrene and alkyl (meth)acrylates from a porphyrin initiator core via ATRP. Macromolecules 2007;40(20):7157–65.
5. Steinschulte AA, Schulte B, Drude N, Erberich M, Herbert C, Okuda J, Möller M, Plamper FA. A nondestructive, statistical method for determination of initiation efficiency: dipentaerythritol-aided synthesis of ternary ABC_3 miktoarm stars using a combined "arm-first" and "core-first" approach. Polym Chem. 2013;4:3885–3895.
6. Wu L, McHale R, Feng G, Wang X. RAFT synthesis and self-assembly of free-base porphyrin cored star polymers. Int J Polym Sci. 2011;2011:1–11.
7. Dai XH, Dong CM, Fa HB, Yan D, Wei Y. Supramolecular polypseudorotaxanes composed of star-shaped porphyrin-cored poly(ε-caprolactone) and α-cyclodextrin. Biomacromolecules 2006;7(12):3527–33.
8. Jia M, Ren T, Wang A, Yuan W, Ren J. Amphiphilic star-shaped poly(e-caprolactone-*block*-poly(L-Lysin) copolymers with porphyrin core: synthesis, self-assembly, and cell viability assay. J Appl Polym Sci. 2014;131:40097.
9. Jin RH. Water soluble star block poly(oxazoline) with porphyrin label: a unique emulsion and its shape direction. J Mater Chem. 2004;14:320–7.
10. Hoogenboom R, Fijten MWM, Kickelbick G, Schubert US. Synthesis and crystal structures of multifunctional tosylates as basis for star-shaped poly(2-ethyl-2-oxazoline)s. Beilstein J Org Chem. 2010;6:773–83.
11. Kolb HC, Finn MG, Sharpless KB. Click chemistry: diverse chemical function from a few good reactions. Angew Chem Int Ed. 2001;40(11):2004–21.
12. Binder WH, Sachsenhofer R. 'Click' chemistry in polymer and materials science. Macromol Rapid Commun. 2007;28(1):15–54.
13. Fournier D, Hoogenboom R, Schubert US. Clicking polymers: a straightforward approach to novel macromolecular architectures. Chem Soc Rev. 2007;36(8):1369–80.
14. Barner-Kowollik C, Du Prez FE, Espeel P, Hawker CJ, Junkers T, Schlaad H, Van Camp W. "Clicking" polymers or just efficient linking: what is the difference? Angew Chem Int Ed. 2011;50(1):60–2.
15. Xi W, Scott TF, Kloxin CJ, Bowman CN. Click chemistry in materials science. Adv Funct Mater. 2014;24(18):2572–90.
16. Espeel P, Du Prez FE. "Click"-inspired chemistry in macromolecular science: matching recent progress and user expectations. Macromolecules 2015;48(1):2–14.
17. Xu LQ, Yao F, Fu GD, Kang ET. Interpenetrating network hydrogels via simultaneous "click chemistry" and atom transfer radical polymerization. Biomacromolecules 2010;11(7):1810–7.
18. Koschella A, Hartlieb M, Heinze T. A "click-chemistry" approach to cellulose-based hydrogels. Carbohyd Polym. 2011;86(1):154–61.
19. Durmaz H, Dag A, Altintas O, Erdogan T, Hizal G, Tunca U. One-pot synthesis of ABC type triblock copolymers via in situ click [3 + 2] and Diels-Alder [4 + 2] reactions. Macromolecules 2007;40(2):191–8.
20. Zhu J, Zhu X, Kang ET, Neoh KG. Design and synthesis of star polymers with hetero-arms by the combination of controlled radical polymerizations and click chemistry. Polymer 2007;48(24):6992–9.
21. Rudolph T, Nunns A, Schwenke AM, Schacher FH. Synthesis and self-assembly of poly(ferrocenyldimethylsilane)-block-poly(2-alkyl-2-oxazoline) block copolymers. Polym Chem. 2015;6:1604–12.
22. Rudolph T, Crotty S, Lühe Mvd, Pretzel D, Schubert US, Schacher FH. Synthesis and solution properties of double hydrophilic poly(ethylene oxide)-block-poly(2-ethyl-2-oxazoline) (PEO-b-PEtOx) star block copolymers. Polymers 2013;5(3):1081–101.
23. Kempe K, Krieg A, Becer CR, Schubert US. "Clicking" on/with polymers: a rapidly expanding field for the straightforward preparation of novel macromolecular architectures. Chem Soc Rev. 2012;41(1):176–91.
24. Sternberg ED, Dolphin D, Brückner C. Porphyrin-based photosensitizers for use in photodynamic therapy. Tetrahedron 1998;54(17):4151–202.
25. Meunier B. Metalloporphyrins as versatile catalysts for oxidation reactions and oxidative DNA cleavage. Chem. Rev. 1992;92(6):1411–56.
26. Li Y, Auras F, Lobermann F, Doblinger M, Schuster J, Peter L, Trauner D, Bein T. A photoactive porphyrin-based periodic mesoporous organosilica thin film. J Am Chem Soc. 2013;135(49):18513–9.
27. Zhamkochyan GA, Akopyan ME, Akopyan LM, Kurtikyan TS. Synthesis of new unsaturated mesotetraarylporphyrins. Chem Heterocycl Compounds 1987;23(2):186–91.
28. Speckbacher M, Yu L, Lindsey JS. Formation of porphyrins in the presence of acid-labile metalloporphyrins: a new route to mixed-metal multiporphyrin arrays. Inorg Chem. 2003;42(14):4322–37.
29. Garate-Morales JL, Reyes-Ortega Y, Alvarez-Toledano C, Gurierrez-Perez R, Ramirez-Rosales D, Zamorano-Ulloa R, Basurto-Uribe E, Hernandez-Diaz J, Contreras R. Spectroscopic studies of novel porphyrin-copper(II) and zinc(II) complexes that share the pinch-porphyrin family structure of iron(III) complex models of peroxidases. Trans Metal Chem. 2002;27(8):906–17.
30. Kumar A, Maji S, Dubey P, Abhilash GJ, Pandey S, Sarkar S. One-pot general synthesis of metalloporphyrins. Tetrahedron Lett. 2007;48(41):7287–90.
31. Rowan SJ, Cantrill SJ, Cousins GRL, Sanders JKM, Stoddart JF. Dynamic covalent chemistry. Angew Chem Int Ed. 2002;41: 898–952.
32. Roberts DA, Schmidt TW, Crossley MJ, Perrier S. Tunable self-assembly of triazole-linked porphyrin-polymer conjugates. Chem Eur J. 2013;19(38):12759–70.
33. Jin RH. Self-assembly of porphyrin-centered amphiphilic star block copolymer into polymeric vesicular aggregates. Macromol Rapid Commun. 2003;204(3):403–9.
34. Jin RH. Controlled location of porphyrin in aqueous micelles self-assembled from porphyrin centered amphiphilic star poly(oxazolines). Adv Mater. 2002;14:889–92.
35. Rudolph T, Kumar Allampally N, Fernández G, Schacher FH. Controlling aqueous self-assembly mechanisms by hydrophobic interactions. Chem Eur J. 2014;20(43):13871–5.
36. Dinçer H, Mert H, Şen BN, Dağ A, Bayraktar S. Synthesis and characterization of novel tetra terminal alkynyl-substituted phthalocyanines and their star polymers via click reaction. Dyes Pigm. 2013;98(2):246–54.
37. Lambermont-Thijs HML, van der Woerdt FS, Baumgaertel A, Bonami L, Du Prez FE, Schubert US, Hoogenboom R. Linear poly(ethylene imine)s by acidic Hydrolysis of poly(2-oxazoline)s: kinetic screening, thermal properties, and temperature-induced solubility transitions. Macromolecules 2009;43(2):927–33.

38. Tauhardt L, Kempe K, Knop K, Altuntaş E, Jäger M, Schubert S, Fischer D, Schubert US. Linear polyethyleneimine: optimized synthesis and characterization – On the way to "Pharmagrade" batches. Macromol Chem Phys. 2011;212:1918–24.
39. de la Rosa VR, Bauwens E, Monnery BD, De Geest BG, Hoogenboom R. Fast and accurate partial hydrolysis of poly(2-ethyl-2-oxazoline) into tailored linear polyethylenimine copolymers. Polym Chem. 2014;5(17):4957–64.
40. Lemon CM, Brothers PJ, Boitrel B. Porphyrin complexes of the period 6 main group and late transition metals. Dalton Trans. 2011;40(25):6591–609.

Supplemental Material: The online version of this article (DOI: 10.1515/epoly-2015-0041) offers supplementary material, available to authorized users.